

Science

AAAS

Multifunctional Carbon Nanotube Yarns by Downsizing an Ancient Technology

Mei Zhang, *et al.*

Science **306**, 1358 (2004);

DOI: 10.1126/science.1104276

The following resources related to this article are available online at www.sciencemag.org (this information is current as of November 16, 2007):

Updated information and services, including high-resolution figures, can be found in the online version of this article at:

<http://www.sciencemag.org/cgi/content/full/306/5700/1358>

Supporting Online Material can be found at:

<http://www.sciencemag.org/cgi/content/full/306/5700/1358/DC1>

This article **cites 14 articles**, 7 of which can be accessed for free:

<http://www.sciencemag.org/cgi/content/full/306/5700/1358#otherarticles>

This article has been **cited by** 61 article(s) on the ISI Web of Science.

This article has been **cited by** 2 articles hosted by HighWire Press; see:

<http://www.sciencemag.org/cgi/content/full/306/5700/1358#otherarticles>

This article appears in the following **subject collections**:

Materials Science

http://www.sciencemag.org/cgi/collection/mat_sci

Information about obtaining **reprints** of this article or about obtaining **permission to reproduce this article** in whole or in part can be found at:

<http://www.sciencemag.org/about/permissions.dtl>

uncertainty in the Cs fountain frequency (1 part in 10^{15} statistical over the time scale of these measurements and 1 part in 10^{15} systematic) (18) and from the uncertainty in correcting for the frequency shifts in the cables used to transfer the maser signal to the femtosecond comb laboratory. Lastly, the uncertainty in the relative altitudes of the Sr ion trap and the Cs fountain leads to a small uncertainty because of the gravitational shift.

Correcting for the systematic shifts gives frequency values of 444,779,044,095,484.3 (1.9) Hz and 444,779,044,095,484.8 (1.6) Hz for the data taken with use of the two different methods of nulling the electric quadrupole shift, which agree to well within their statistical uncertainties. The unweighted mean of the two values gives a final value for the 674-nm electric quadrupole clock transition frequency in $^{88}\text{Sr}^+$ of 444,779,044,095,484.6 (1.5) Hz. In calculating the final uncertainty, only the statistical error is reduced, because the systematic uncertainties are mostly common to the two measurements. This result is in good agreement with earlier, less-accurate measurements (9, 10) of the Sr clock transition frequency. It is also a factor of 3 more accurate than any previously reported optical frequency measurement, and its fractional uncertainty of 3.4×10^{-15} is within a factor of 3 of that of the NPL primary Cs standard (when both statistical and systematic errors

are considered). Apart from the uncertainty arising from the Cs standard, the dominant sources of uncertainty in our measurement are technical in nature and can be reduced by refinements to the experimental arrangement. In particular, improvements to the extinction of the cooling laser radiation during the probe laser periods (e.g., by placing an iris after the shutter) will reduce the 422-nm ac Stark shift, whereas reductions in the probe laser linewidth and ULE cavity drift rate will reduce servo errors. A second endcap trap is also being developed, which will enable a more detailed investigation of systematic errors by means of two-trap comparisons. With these improvements, we anticipate a frequency measurement that is limited by the accuracy of the Cs fountain. As well as being of interest for a possible future redefinition of the second, measurements of this and other optical frequency standards over timescales of a few years will provide increasingly sensitive laboratory tests of the time invariance of fundamental constants (22, 23).

References and Notes

1. P. Gill, Ed., *Proceedings of the 6th Symposium on Frequency Standards and Metrology* (World Scientific, Singapore, 2002).
2. R. J. Rafac et al., *Phys. Rev. Lett.* **85**, 2462 (2000).
3. S. A. Diddams et al., *Science* **293**, 825 (2001); published online 12 July 2001 (10.1126/science.1061171).

4. T. Udem, J. Reichert, R. Holzwarth, T. W. Hänsch, *Opt. Lett.* **24**, 881 (1999).
5. S. A. Diddams et al., *Phys. Rev. Lett.* **84**, 5102 (2000).
6. J. Stenger, C. Tamm, N. Haverkamp, S. Weyers, H. R. Telle, *Opt. Lett.* **26**, 1589 (2001).
7. P. J. Blythe et al., *Phys. Rev. A* **67**, 020501(R) (2003).
8. T. Becker et al., *Phys. Rev. A* **63**, 051802(R) (2001).
9. H. S. Margolis et al., *Phys. Rev. A* **67**, 032501 (2003).
10. A. A. Madej, J. E. Bernard, P. Dubé, L. Marmet, R. S. Windeler, *Phys. Rev. A* **70**, 012507 (2004).
11. T. Udem et al., *Phys. Rev. Lett.* **86**, 4996 (2001).
12. C. A. Schrama, E. Peik, W. W. Smith, H. Walther, *Opt. Commun.* **101**, 32 (1993).
13. I. Siemers, M. Schubert, R. Blatt, W. Neuhauser, P. E. Toschek, *Europhys. Lett.* **18**, 139 (1992).
14. D. J. Berkeland, J. D. Miller, J. C. Bergquist, W. M. Itano, D. J. Wineland, *J. Appl. Phys.* **83**, 5025 (1998).
15. R. W. P. Drever et al., *Appl. Phys. B* **31**, 97 (1983).
16. H. Dehmelt, *IEEE Trans. Instrum. Meas.* **31**, 83 (1982).
17. G. P. Barwood, H. S. Margolis, G. Huang, P. Gill, H. A. Klein, *Phys. Rev. Lett.* **93**, 133001 (2004).
18. K. Szymaniec, W. Chalupczak, P. B. Whibberley, S. N. Lea, D. Henderson, in preparation.
19. W. M. Itano, *J. Res. Natl. Inst. Stand. Technol.* **105**, 829 (2000).
20. P. Dubé, L. Marmet, A. A. Madej, J. E. Bernard, presentation at the 2004 Conference on Precision Electromagnetic Measurements, London, 27 June to 2 July 2004.
21. J. E. Bernard, L. Marmet, A. A. Madej, *Opt. Commun.* **150**, 170 (1998).
22. M. Fischer et al., *Phys. Rev. Lett.* **92**, 230802 (2004).
23. E. Peik et al., *Phys. Rev. Lett.* **93**, 170801 (2004).
24. We thank W. Chalupczak, D. Henderson, P. Stacey, and P. Whibberley for their contributions to the caesium fountain and hydrogen maser operation. This work was supported by the Department of Trade and Industry National Measurement System Length program under contract LE02/A01.

21 September 2004; accepted 25 October 2004

Multifunctional Carbon Nanotube Yarns by Downsizing an Ancient Technology

Mei Zhang,¹ Ken R. Atkinson,² Ray H. Baughman^{1*}

By introducing twist during spinning of multiwalled carbon nanotubes from nanotube forests to make multi-ply, torque-stabilized yarns, we achieve yarn strengths greater than 460 megapascals. These yarns deform hysteretically over large strain ranges, reversibly providing up to 48% energy damping, and are nearly as tough as fibers used for bulletproof vests. Unlike ordinary fibers and yarns, these nanotube yarns are not degraded in strength by overhand knotting. They also retain their strength and flexibility after heating in air at 450°C for an hour or when immersed in liquid nitrogen. High creep resistance and high electrical conductivity are observed and are retained after polymer infiltration, which substantially increases yarn strength.

Archaeological evidence from the late Stone Age indicates that humans long ago discovered the basic secrets of spinning (1). Similar processes involving the twisting of centimeter-long fibers to make continuous yarns are critically important for many of today's industries, and they remain a focus of research and development. The present work reduces the diameters of fibers used for spinning by a factor of 1000, increases twist by about the same factor, and discovers

useful properties for the resulting spun carbon nanotube yarns.

Nanotube spinning is motivated in part by interest in the very high strength and electrical and thermal conductivities of individual nanotubes (2). Breakthroughs have been made in wet spinning of single-walled nanotubes (SWNTs) (3–6) and in dry-state spinning of multiwalled nanotubes (MWNTs) and SWNTs (7, 8), but the highest strength achieved with any of these spinning methods

is about an order of magnitude lower than the strength of individual SWNTs, ~37 GPa (2).

There is no single best solution to the challenge of converting available nanotube powders into useful fibers and yarns. Excellent fiber strength (4.2 GPa) and modulus (167 GPa) have been achieved by incorporating SWNTs in a high-strength, high-modulus polymer, but electrical and thermal conductivities are low because of limitations on nanotube content (5). Much higher conductivities result for thermally annealed, solution-spun yarns comprising only SWNTs (2, 4), but achieved mechanical properties are far lower than can be obtained using a polymer matrix for intertube stress transfer (6). Coagulation-spun yarns comprising ~60 weight % SWNTs in a polymer matrix have high strength (~1.8 GPa) and more than 10 times the toughness (~600 J/g) of any synthetic polymer, but the electrical conductivity is so low that charge/discharge rates for fiber-based supercapacitors are limited (6). The challenge is to produce yarns that are at the same time strong, creep resistant, highly

¹NanoTech Institute and Department of Chemistry, University of Texas at Dallas, Richardson, TX 75083, USA. ²CSIRO Textile & Fibre Technology, P.O. Box 21, Belmont, Victoria 3216, Australia.

*To whom correspondence should be addressed. E-mail: ray.baughman@utdallas.edu

conducting, and reversibly deformable over relatively large strains to absorb energy.

It is likely that the characteristics of the frictional forces that couple fibers in twist-based yarns change as fiber diameter decreases to the nanoscale. Nevertheless, a generic equation (9) provides useful insights for spinning nanotube yarns. Specifically, the ratio of yarn tensile strength (σ_y) to the tensile strength of the component fibers (σ_f) is approximately

$$\sigma_y/\sigma_f \approx \cos^2 \alpha [1 - (k \operatorname{cosec} \alpha)] \quad (1)$$

where $k = (dQ/\mu)^{1/2}/3L$, α is the helix angle that fibers make with the yarn axis, d is the fiber diameter, μ is the friction coefficient between fibers, L is the fiber length, and Q is the fiber migration length (i.e., the distance along the yarn over which a fiber shifts from the yarn surface to the deep interior and back again).

The $\cos^2 \alpha$ term in Eq. 1 describes the strength decrease of a twisted assembly of continuous fibers, which occurs because the fibers in the twisted yarn are inclined at the angle α with respect to the tensile axis. For short fibers, however, in the absence of twist there is little strength because there are no significant transverse forces to bind the fiber assembly together. The $[1 - (k \operatorname{cosec} \alpha)]$ term describes the generation of transverse forces by transfer of the tensile load to the yarn surface, which locks the fibers together as a coherent structure. The components of k show that the strength obtainable for a given level of twist increases with increasing coefficient of friction and fiber length and with decreasing fiber diameter and fiber migration length.

Like the spinning method of Jiang *et al.* (7), the present process involves drawing carbon nanotubes from a MWNT “forest” (in which all nanotubes grow from a substrate in a manner resembling tree trunks in a dense bamboo forest and have nearly the same height). Li *et al.* (8) made the important discovery that MWNT yarns with much higher strengths could be directly spun from aerogels during nanotube synthesis by chemical vapor deposition (CVD). Although a stable twisted yarn was shown (8), the ratio of nanotube length ($\sim 30 \mu\text{m}$) to yarn diameter was very low (about unity), which should limit the benefits of twisting.

Scanning electron microscope (SEM) images (Fig. 1, A and B) show yarn assembly during our spinning process, in which MWNTs ~ 10 nm in diameter are simultaneously drawn from the MWNT forest and twisted. The direction of drawing was orthogonal to the original nanotube direction and parallel to the substrate, although the spinning process is sufficiently robust that the angle between the initial nanotube direction and the draw direction can be decreased from 90° to almost 0° . The nanotube forests were grown on an iron catalyst-coated substrate by CVD, using a method (10) that builds on important

advances of the Dai (11) and Ren (12) groups. Although this spinning process is amenable to automation for spinning continuous yarns, the present results are for yarns that were hand-drawn from a nanotube forest while they were twisted with a variable-speed motor operating at ~ 2000 rpm (13). In some spinning trials, the spun yarns had such small diameters ($\sim 1 \mu\text{m}$) that spinning was somewhat like hauling in a fish with an invisible line—with the additional complication that the line is simultaneously being twisted at a high rate. The achieved yarn length was limited to ~ 1 m by the arm length of the person doing the drawing, although there is no fundamental limit on achievable yarn lengths.

Although the MWNT lengths are 0.1 to 1% those of staple fibers such as wool and cotton, this simple method results in yarns that are strong, very flexible, tough, and highly conducting. The geometry of the spun yarn resembles that of wool or cotton yarn, and we were able to select spinning parameters by extending the classic theory of staple yarns from the microscale to the nanoscale (9), using additional insights from theoretical work on nanotubes by the Pipes and Ruoff groups (14, 15).

The yarn diameter was set by controlling the width of the forest sidewall that was used to generate an initial wedge-shaped ribbon, which is shown converging from about the thickness of the forest to that of the yarn at the apex (Fig. 1) (fig. S2). The forest sidewall width ranged from less than $150 \mu\text{m}$ to ~ 3 mm; the resulting unplied yarn diameters were between ~ 1 and $10 \mu\text{m}$. A forest sidewall

$200 \mu\text{m}$ wide produced a twisted yarn $\sim 2 \mu\text{m}$ in diameter, and a forest area of 1 cm^2 could generate an estimated 50 m of this yarn. The inserted twist was typically $\sim 80,000$ turns/m, versus ~ 1000 turns/m for a highly twisted conventional textile yarn with diameter 80 times as large. Because $\tan \alpha/\pi D$ is the twist required to provide the helix angle α for a yarn having diameter D , such huge twists provide helix angles comparable to those of highly twisted conventional textiles.

Measurements of yarn diameter by SEM and yarn mass per length showed that the twisted yarn had a density of $\sim 0.8 \text{ g cm}^{-3}$. The linear density of the unplied yarns (called “singles”) was typically $\sim 10 \mu\text{g m}^{-1}$, compared with the usual 10 mg m^{-1} and 20 to 100 mg m^{-1} for cotton and wool yarns, respectively. About 100,000 MWNTs pass through the cross section of a nanotube yarn $5 \mu\text{m}$ in diameter, as compared with the 40 to 100 fibers in the cross section of typical commercial wool (worsted) and cotton yarns.

SEM images of singles, two-ply, and four-ply MWNT yarns, respectively, are shown in Fig. 2, A to C. The two-ply yarns were obtained by overtwisting a singles yarn and then allowing it to relax (untwist) around itself until it reached a torque-balanced state. This procedure was repeated for the two-ply yarn, using an opposite twist direction, to produce four-ply yarns; such a method was used to make rope in the days of sailing vessels. The two-ply structure was torque balanced, as indicated by MWNT alignment along the yarn axis (Fig. 2B).

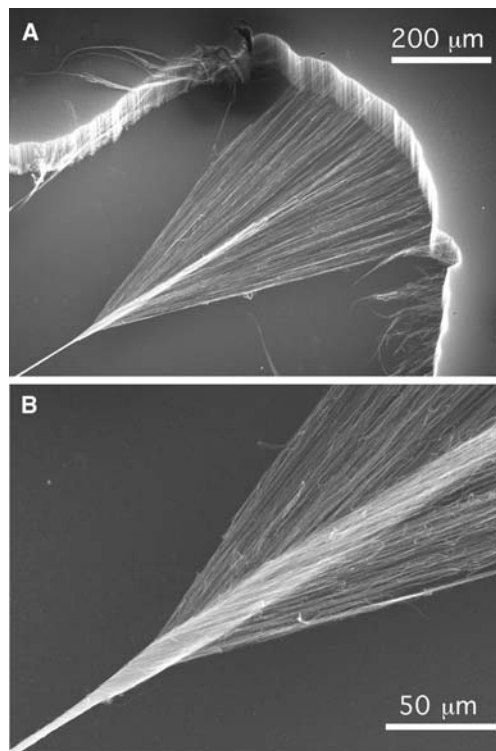


Fig. 1. (A and B) SEM images, at two different magnifications, of a carbon nanotube yarn in the process of being simultaneously drawn and twisted during spinning from a nanotube forest outside the SEM. The draw twist process was interrupted and the sample was transferred to a SEM for image recording. A forest strip (width $\sim 600 \mu\text{m}$) formed the pictured twisted yarn, $3.2 \mu\text{m}$ in diameter (fig. S2). The MWNTs, ~ 10 nm in diameter with length 10,000 times their width, form small bundles of a few nanotubes each in the forest, with individual nanotubes moving in and out of different bundles. The three-dimensional connectivity caused by intermittently switched bundling, visible in SEM micrographs, is believed to be important for the spinning process.

Unlike singles yarn of a conventional textile, the MWNT singles yarn largely retains twist when the yarn ends are released. The enhanced locking of twist possibly reflects the high interfiber contact area per yarn volume as a result of the very high surface-to-volume ratio of the MWNTs. Particularly surprising is the observation that twist is retained up to the location of the break point for singles yarns that have been broken by tensile extension. In part because of twist retention, highly twisted singles yarns can be knitted and knotted (Fig. 2, D and E). Abrasion and knotting, especially with an overhand knot, seriously degrades the strength of most polymer fibers (including those used for antiballistic vests), conventional textile yarns, individual polymer chains, actin filaments, and DNA, causing rupture at the entrance to the knot (16, 17). This is not the case for the investigated singles and two-ply nanotube yarns, where tensile failure is not observed in the vicinity of an inserted overhand knot. High abrasion resistance is suggested by the absence of ultimate tensile failure in a long yarn loop that was pulled through a very tight overhand knot. This useful resistance to knot-induced failure is likely a consequence of the very small tensile and compressive strains introduced by bending a MWNT 10 nm in diameter to the radius of a yarn knot; these strains are 0.05% of those that would occur in a fiber 20 μm in diameter with the same bending radius.

Although very high electrical conductivities have been observed for yarns of pure nanotubes (4, 7, 8), continuous composite fibers involving nanotubes and insulating polymers generally have low conductivities, whether the polymer is present during the spinning process or added after spinning. We find that the intertube mechanical coupling introduced by twisting largely maintains electronic connectivity between nanotubes during infiltration (18) of poly(vinyl alcohol) (PVA), thereby avoiding a major decrease in electrical conductivity. The investigated yarns (diameters from 2 to 10 μm) had a four-probe electrical conductivity of ~ 300 S/cm at room temperature and a negative temperature dependence of resistance ($\sim -0.1\%$ per $^{\circ}\text{C}$ between liquid nitrogen and room temperature). PVA infiltration decreased yarn electrical conductivity by only $\sim 30\%$, leading to MWNT/PVA composite yarns whose electrical conductivity is more than 150 times that of coagulation-spun nanotube composite fibers (6) containing this insulating polymer.

The untwisted yarns were so weak that they broke when pulled away from surfaces that they accidentally contacted, whereas the singles yarns had measured tensile strengths between 150 and 300 MPa (13). Higher strengths, between 250 and 460 MPa, were observed for two-ply yarns. These values are

engineering stresses based on cross-sectional area measured by SEM for the unstressed yarn. As a result of a giant Poisson's ratio effect, the true stress at break (normalized to the true cross-sectional area at the beginning of yarn rupture) is $\sim 30\%$ larger. From the maximum observed density of 0.8 g cm^{-3} , we calculate the density-normalized failure stress of the two-ply yarns to be between 310 and 575 MPa/g $\cdot\text{cm}^{-3}$, as compared with values between 50 and 500 MPa/g $\cdot\text{cm}^{-3}$ for polymer-free nanotube fiber spun from an aerogel (8) and >3 GPa/g $\cdot\text{cm}^{-3}$ for the highest performance graphite fibers (19). Infiltration with PVA (18) increased the observed strengths of singles yarns to 850 MPa.

The pure nanotube yarns had a much larger strain-to-failure (up to 13%) than graphite fibers ($\sim 1\%$). This high failure strain, combined with high failure strength, meant that the work needed to break the yarns (called toughness) was also high: ~ 14 J/g for the singles yarn, 20 J/g for the two-ply yarn, and 11 J/g for the PVA-infiltrated singles yarns, which combined their higher strength with a lower strain-to-failure (~ 3 to 4%). Although this toughness for the two-ply yarn (20 J/g) is above that of graphite fibers (12 J/g) and approaches that of commercial fibers used for antiballistic vests (~ 33 J/g for Kevlar fibers), far greater toughness has been demonstrated (6) for solution-spun SWNT/PVA composite fibers (600 J/g).

The stress-strain curves (Fig. 3A) show rapid collapse of the yarn stress once the

breaking strain is exceeded, as also seen for conventional yarns (9). A simple model of tensile failure is thought to apply: Initial failure of the MWNTs in a central zone increases the freedom of movement of the MWNTs in the surrounding zones, which reduces transverse forces and ultimately leads to sliding of nanofibers with respect to each other (drafting) and catastrophic failure of the yarn. This process ensures that the ends of the broken yarn are drafted, as we observed.

The nanotube yarns showed hysteretic stress-strain curves when subjected to load-unload cycles (Fig. 3B). Although complete unloading did not return the yarn to its original length, the initial hysteresis loop was essentially unshifted on subsequent cycles. Depending on initial strain, the observed energy loss per stress-strain cycle of a two-ply MWNT yarn was 9 to 22% for cycle strain of 0.5%, 24 to 28% for cycle strain of 1.5% (Fig. 3C), and 39 to 48% for the maximum reversible cycle strain (2 to 3% for total strains up to 8%). Within a hysteresis loop, the effective modulus on initial unloading and initial reloading was much larger than for the final parts of the unloading and reloading steps (Fig. 3D). Also relevant for applications, the failure strength of nanotube yarn (singles and two-ply) was unaffected by 50 loading-unloading cycles over a stress range of 50% of the failure stress. The nanotube yarns were resistant to creep and associated stress relaxation: The stress relaxed no more than 15% when a two-ply nanotube yarn was held for 20 hours at 6% strain (initial

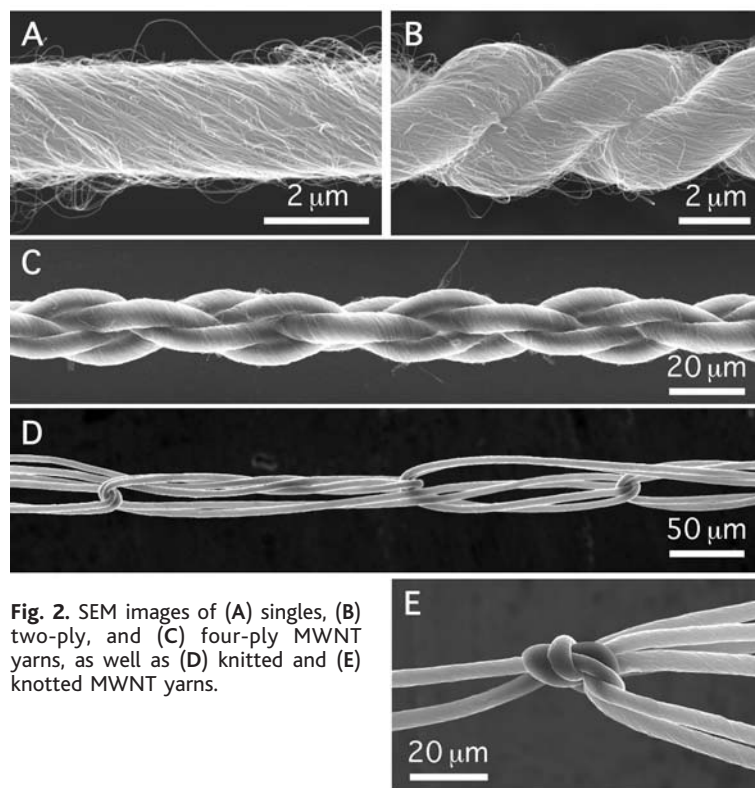


Fig. 2. SEM images of (A) singles, (B) two-ply, and (C) four-ply MWNT yarns, as well as (D) knitted and (E) knotted MWNT yarns.

stress 170 MPa), and this small stress relaxation occurred within the first 20 min and was largely viscoelastic. Thermal stability was also high: The failure strength of a two-ply yarn (300 MPa) was essentially unchanged after heating in air at 450°C for an hour. Although air oxidation was evident in SEM micrographs, a nanotube yarn held at 450°C for 10 hours was sufficiently strong and flexible to be tightly knotted. Tight knot tying was also possible while the nanotube yarn was immersed in liquid nitrogen.

We observed giant Poisson's ratios for the nanotube yarns, which increased with increasing strain from 2.0 to 2.7 for MWNT singles yarn and from 3.3 to 4.2 for two-ply yarn (Fig. 3E). This Poisson's ratio of 4.2 means that elongating the yarn by a strain ϵ provides a strain of -4.2ϵ in each of the lateral dimensions and a fractional volume decrease of 7.4ϵ , versus a fractional volume increase of $\sim 0.4 \epsilon$ for an ordinary solid with a typical Poisson's ratio of ~ 0.3 .

The origin of these giant Poisson ratios is topological and is basically the same as for "finger trap" toys, selenium and tellurium single crystals, and the helically wound muscular hydrostats that provide stiffness for squid tentacles and the bodies of various worms (20). Unwinding an ideal helix by stretching provides a Poisson's ratio of >0.5 and stretch densification as long as the helix angle is sufficiently small ($<54.73^\circ$). Hearle (21) long ago predicted giant Poisson's ratios for conventional yarns when this helix angle α is small and the ratio of fiber tensile modulus to yarn bulk modulus is large, and Poisson's ratios of up to 0.8 have been predicted by Pipes and Hubert (14) for twisted nanotube arrays. These Poisson's ratios, and the associated stretch-induced densification of up to 7.4 ϵ , might be used for tuning the absorption and permeability of nanotube yarns and textiles by applying small applied strains in a yarn direction.

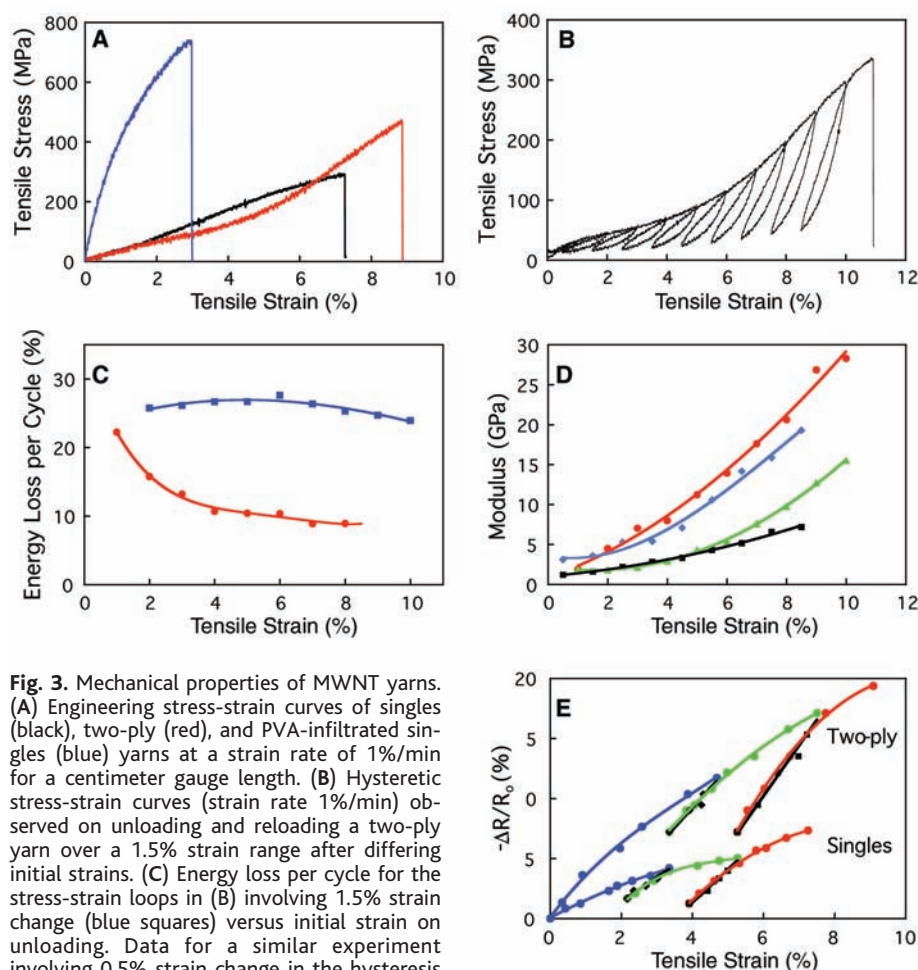


Fig. 3. Mechanical properties of MWNT yarns. (A) Engineering stress-strain curves of singles (black), two-ply (red), and PVA-infiltrated singles (blue) yarns at a strain rate of 1%/min for a centimeter gauge length. (B) Hysteretic stress-strain curves (strain rate 1%/min) observed on unloading and reloading a two-ply yarn over a 1.5% strain range after differing initial strains. (C) Energy loss per cycle for the stress-strain loops in (B) involving 1.5% strain change (blue squares) versus initial strain on unloading. Data for a similar experiment involving 0.5% strain change in the hysteresis loops are also shown (red circles). (D) Effective yarn moduli calculated for the stress-strain loops shown in (B) versus total tensile strain. Red circles and black squares are the effective moduli for the beginning and end of unloading, respectively; blue diamonds and green triangles are those for the beginning and end of reloading, respectively. (E) Percent change in diameter and length of a two-ply yarn (top) and a singles yarn (bottom) measured during yarn stretching in a SEM. Symbols: blue circles, initial stretch; black diamonds, first stress decrease; green circles, second stress increase; black squares, second stress decrease; red circles, stress increase until yarn rupture. Curves in (C) to (E) are guides for the eye.

The MWNT yarns are interesting as multifunctional materials. Their strength, toughness, mechanical energy damping capability, and resistance to knot-induced failure could be exploited, as could yarn diameters that are 2% the diameter of a human hair. Replacing metal wires in electronic textiles with these nanotube yarns could provide important new functionalities, such as the ability to actuate as an artificial muscle and to store energy as a fiber supercapacitor or battery. The small yarn diameters, like those of micro-denier yarns used for soft fabrics, could eliminate the uncomfortable rigidity sometimes found for metal wire-containing conducting textiles that provide radio or microwave absorption, electrostatic discharge protection, textile heating, or wiring for electronic devices.

References and Notes

1. E. J. W. Barber, *Prehistoric Textiles* (Princeton Univ. Press, Princeton, NJ, 1992).
2. R. H. Baughman, A. A. Zakhidov, W. A. de Heer, *Science* **297**, 787 (2002).
3. B. Vigolo et al., *Science* **290**, 1331 (2000).
4. L. M. Ericson et al., *Science* **305**, 1447 (2004).
5. S. Kumar et al., *Macromolecules* **35**, 9039 (2002).
6. A. B. Dalton et al., *Nature* **423**, 703 (2003).
7. K. Jiang, Q. Li, S. Fan, *Nature* **419**, 801 (2002).
8. Y. Li, I. A. Kinloch, A. H. Windle, *Science* **304**, 276 (2004).
9. J. W. S. Hearle, P. Grosberg, S. Backer, *Structural Mechanics of Fibers, Yarns, and Fabrics*, vol. 1 (Wiley, New York, 1969).
10. Aligned nanotube forests comprising MWNTs ~ 8 to ~ 15 nm in diameter were synthesized in a quartz tube 45 mm in diameter by atmospheric-pressure CVD of 5 mol % C_2H_2 in He at 680°C, at a total flow rate of 580 sccm for 10 min. The catalyst was an iron film, 5 nm thick, that was deposited on a Si wafer substrate by electron beam evaporation. SEM and thermal gravimetric measurements indicated that the purity of the spun yarns was very high (~ 96 to 98% C in the form of MWNTs), with 2 to 4% Fe and amorphous carbon. No carbon particles were observed.
11. S. Fan et al., *Science* **283**, 512 (1999).
12. Z. F. Ren et al., *Science* **282**, 1105 (1998).
13. See supporting data on Science Online.
14. R. B. Pipes, P. Hubert, *Compos. Sci. Technol.* **62**, 419 (2002).
15. D. Qian, W. K. Liu, R. S. Ruoff, *Compos. Sci. Technol.* **63**, 1561 (2003).
16. A. M. Saitta, P. D. Soper, E. Wasserman, M. L. Klein, *Nature* **399**, 46 (1999).
17. Y. Arai et al., *Nature* **399**, 446 (1999).
18. MWNT/PVA composite yarns were made either by soaking a singles yarn for 15 hours in 5 wt % aqueous PVA solution or by passing a singles yarn through a drop of this solution during spinning, and then drying. The molecular weight of the PVA was in the range 77,000 to 79,000, and it was 99.0 to 99.8% hydrolyzed.
19. J.-B. Donnet, *Carbon Fibers* (Dekker, New York, 1998).
20. R. H. Baughman, S. Stafström, C. Cui, S. O. Dantas, *Science* **279**, 1522 (1998).
21. J. W. S. Hearle, *J. Polym. Sci. C* **20**, 215 (1967).
22. We thank the staff of the University of Texas at Dallas NanoTech Institute and clean room for their assistance. Supported by Defense Advanced Research Projects Agency/U.S. Army Research Office grant W911NF-04-1-0174, Texas Advanced Technology Program grant 009741-0130-2003, and the Robert A. Welch Foundation.

Supporting Online Material

www.sciencemag.org/cgi/content/full/306/5700/1358/DC1
Materials and Methods
Figs. S1 and S2

19 August 2004; accepted 22 October 2004